Protection and Control of Modern Power Systems

ORIGINAL RESEARCH Open Access

A direct power control of a DFIG based-WECS during symmetrical voltage dips

Sara Mensou[1*], Ahmed Essadki[1], Tamou Nasser[2] and Badr Bououlid Idrissi[3]

Abstract

The Wind Energy Conversion System (WECS) based Doubly Fed Induction Generator (DFIG) has experienced a rapid development in the world, which leads to an increasing insertion of this source of energy in the electrical grids. The sudden and temporary drop of voltage at the network can affect the operation of the DFIG; the voltage dips produce high peak currents on the stator and rotor circuits, without protection, the rotor side converter (RSC) will suffer also from over-current limit, consequently, the RSC may even be destroyed and the generator be damaged. In this paper a new Direct Power Control (DPC) method was developed, in order to control the stator powers and help the operation of the aero-generator during the faults grid; by injecting the reactive power into the network to contribute to the return of voltage, and set the active power to the optimum value to suppress the high peak currents. The DPC method was designed using the nonlinear Backstepping (BS) controller associated with the Lyapunov function to ensure the stability and robustness of the system. A comparison study was undertaken to verify the robustness and effectiveness of the DPC-BS to that of the classical vector control (VC) using Proportional-Integral (PI) correctors. All were simulated under the Simulink® software.

Keywords: Wind energy, Doubly-fed induction aero-generator, Voltage dips, DPC strategy, Backstepping technique, Lyapunov function

1 Introduction

The evolution of renewable energy is the best solution to protect the environment and reduces the pollution caused by nuclear energy and fossil resources, renewable energy sources come from: wind energy, sun, geothermal, biomass, marine energy and hydroelectric. Among these sources of energy, the wind energy is the cleanest, effective and promising resource; it's a sustainable way to produce electricity without warming emissions [1, 2], that leads to an increasing insertion in the electrical networks.

The most installed machine in wind farms is the doubly-fed induction generator (DFIG) and the permanent magnet synchronous generator (PMSG). Actually, the DFIG is the widely generator employed because it presents several advantages [3–5] the power electronics converters connecting between the network and the rotor use a part of the total rated power, typically about (30%), which reduces the costs and loss, and it has the flexibility for controlling the reactive and active powers independently, in addition, the operating on the variable speed makes possible to maximize the efficiency of the energy produced. The structure of a doubly-fed induction aero-generator is presented in Fig. 1. In this topology, the stator windings are directly linked to the electrical grid, and the rotor windings are linked the network via a back-to-back power electronic converter, which is placed a DC bus voltage, where the derived name of 'doubly fed' [2].

DFIG is a highly nonlinear system, so several control strategies have been examined to improve the DFIG operation under disturbances [6–11]. Among these control techniques, the most used one is the classical control based on the proportional-integral (PI) correctors, it's very used for it reliability and simplicity of implementation, but its performance degrades when the internal generator parameters varied [12, 13]. In work [6], a nonlinear MPPT control of a DFIG based on feedback linearization control (FLC) was designed, and the stability of the system was achieved using Lyapunov theory.

* Correspondence: sara.mensou11@gmail.com
[1]Research Center of Engineering and Health Sciences and Technologies from ENSET, Mohammed V University, Rabat, Morocco
Full list of author information is available at the end of the article

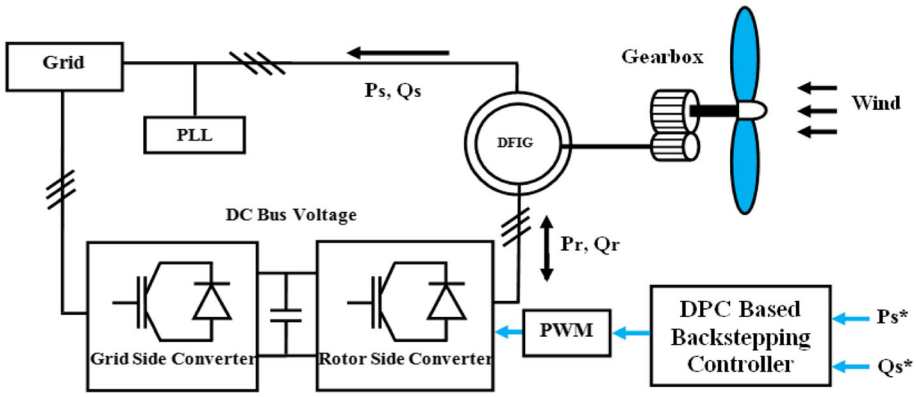

Fig. 1 Structure of wind energy Conversion system based on a DFIG

In reference [7], to enhance the power stability of a DFIG using in wind energy, a sliding mode controller based perturbation observer was designed. Paper [8], propose a novel perturbation estimation based robust state feedback control in order to achieve MPPT of the DFIG, the results obtained was verified by simulation and compared whit other classical methods.

The voltage dip is a temporary and sudden drop of the amplitude from 10% to 90% of the RMS voltage affecting one or more phases at a point in the electrical network; it is characterized by two parameters: the amplitude and duration [13]. Previously, when faults grid occurs, the system protection turns-off and disconnects the generator from the network to protect the aero-generators, which implies a loss of production for several minutes. In this context, the new grid codes require the generator to continue the production of electricity and remain connected to the grid during the faults [14, 15]. Figure 2 presents the limits supported by the wind system during voltage dips in some countries, above the critical line limited and determined by the grid code, the wind turbines must remain connected and should contribute to the return of voltage to it rated value, the capability of

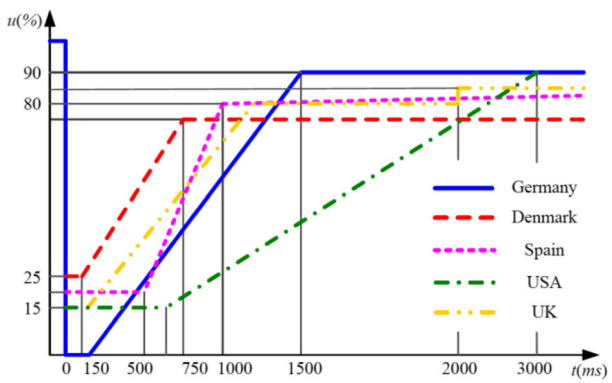

Fig. 2 Limits zone supported by the wind system during voltage dips in some countries

the WECS to stay connected to the network during the period of the voltage drops is called Low Voltage Ride-Through (LVRT) capability.

As the stator windings of the DFIG are linked directly to the network, when severe voltage drop occurs, high peak currents appear on the stator windings, due to the coupling between the stator and rotor circuit, over currents appear on the rotor winding then the rotor side converter (RSC), which leads to increases the voltage in the DC bus capacitor [16] and the oscillations on the torque, consequently, if no protection measurements were installed, the high currents transient can destroy the rotor side converter and the generator [17]. So to protect the system and keep the DFIG connected to the grid during the period of the fault, several control strategies have been proposed and studied in the literature [6–11, 14–27], these control strategies propose using a hardware protective devices or improving control methods.

The crowbar circuits protection are the most popular solution, the principle of this technology, is to connect directly a resistance bank to the rotor of the DFIG when voltage sag is detected, and the doubly-fed induction generator becomes likes a squirrel cage machine [3, 18, 19], that make the generator consumes more reactive power, which leads to voltage instability [20]. This solution limits the high current transient and protects the power converter, but the controllability of the generator becomes impossible [17], so the control of reactive power is lost under the crowbar operation. Another alternative was proposed to compensate the reactive power in [21–23] is the use of the Static Synchronous Compensator (STATCOM) in the WECS, this solution works well but it is very expensive; consequently, it increases the costs.

Alternatively, many control methods have been developed and proposed; in [16, 18] and [24] a DPC was developed to control the stator powers of the DFIG during the voltage sags, the proposed control strategy was verified by laboratory experiments. In [15] a stator flux control method based on the Active Disturbance Rejection

Control (ADRC) corrector was applied to maintain the magnetization of the DFIG during the voltage drop associated whit the crowbar devices, this method work well, but when the crowbars were activated the DFIG control is lost. The stator current control loop using the Proportional and Integral (PI) correctors was proposed in [25], this control strategy was verified and validated by experiments. The conventional and modified vector control approach based on PI correctors was investigated in [26], to ensure the continuity of service of the WECS during the voltage sags, this method was verified by simulation, but the robustness of PI corrector degrades when the internal parameters of the machine are subject to variation. Paper [27] proposes a direct power control (DPC) method based on the sliding mode control (SMC) during a Low Voltage Ride-Through (LVRT), a satisfactory simulation results were achieved.

In this work, we develop a new Direct Power Control (DPC) strategy using the nonlinear Backstepping technique to help the operation of the system, ensure the continuity of service, and the connection to the network during and after the symmetrical voltage dips. The direct powers control objectives: control the active and reactive stator powers of the generator during the faults: the active stator power is controlled to suppress the high peak currents on the stator and rotor circuit, and the reactive power is controlled to contribute to the return of the voltage at the nominal value. The DPC was developed using the doubly-fed induction generator mathematical model, The Backstepping controller was designed from the rotor voltage equations, and the references voltages values are expressed as a function of the stator powers and its errors, during the voltages dips the stator flux is considering variants. In order to validate and analyze our proposed strategy, the aero-generator dynamic model of a rated power of 1.5 kW and DPC-based Backstepping approach were implemented, simulated, and compared whit VC control under symmetrical voltage dips using Simulink® environment.

This research paper is presented as the following sections; section 2, the doubly fed induction generator mathematical model and its behavior under symmetrical fault grid were presented. The direct power control based-Backstepping technique is developed in section 3. In section 4 the simulations results of the system are discussed and analyzed. Finally, some conclusions are given in section 5.

2 Doubly-fed induction generator under voltage dips

2.1 Modeling of the DFIG

The doubly fed-induction generator is modeled in the Park reference frame (d-q) axis. In this section, the stator voltage is oriented along the (q) axis. Hence, the stator and rotor voltages equations can be expressed as the following form [14–16]:

$$V_{s,dq} = V_{sq} = R_s I_{s,dq} + \frac{d\phi_{s,dq}}{dt} \pm \phi_{s,qd}\omega_s \tag{1}$$

$$V_{r,dq} = R_r I_{r,dq} + \frac{d\phi_{r,dq}}{dt} \pm \phi_{r,qd}\omega_r \tag{2}$$

The expressions of the stator and rotor flux of the DFIG as a function of the stator and rotor currents are giving by the following equations:

$$\phi_{s,dq} = L_s I_{s,dq} + L_m I_{r,dq} \tag{3}$$

$$\phi_{r,dq} = L_r I_{r,dq} + L_m I_{s,dq} \tag{4}$$

Using the expressions of the rotor and stator flux (3) and (4), the currents expression becomes:

$$I_{s,dq} = \frac{1}{\sigma L_s}\phi_{s,dq} - \frac{k_r}{\sigma L_s}\phi_{r,dq} \tag{5}$$

$$I_{r,dq} = \frac{1}{\sigma L_r}\phi_{r,dq} - \frac{k_s}{\sigma L_r}\phi_{s,dq} \tag{6}$$

Where: $\sigma = 1 - \frac{L_m^2}{L_s L_r}$, $k_s = \frac{L_m}{L_s}$, $k_r = \frac{L_m}{L_r}$.

The electromagnetic torque of the generator as a function of the stator flux and the rotor current:

$$T_{em} = p\frac{L_m}{L_s}\left(\phi_{sq} I_{rd} - \phi_{sd} I_{rq}\right) \tag{7}$$

The apparent stator power of the doubly fed-induction generator is expressed us:

$$\overline{S_s} = P_s + jQ_s \tag{8}$$

Where the active and the reactive powers are giving by:

$$\begin{cases} P_s = V_{sd} I_{sd} + V_{sq} I_{sq} \\ Q_s = V_{sq} I_{sd} - V_{sd} I_{sq} \end{cases} \tag{9}$$

The subscripts r and s represent the rotor and stator quantities respectively.

In order to study and analyze the behavior of the DFIG under voltage dips, we present the stator and rotor voltages equations in the static reference frame oriented to stator [28]:

$$\overrightarrow{V_s} = R_s \overrightarrow{I_s} + \frac{d\overrightarrow{\phi_s}}{dt} \tag{10}$$

$$\overrightarrow{V_r} = R_r \overrightarrow{I_r} + \frac{d\overrightarrow{\phi_r}}{dt} - \overrightarrow{\phi_r}\omega \tag{11}$$

Using Eqs. (3) and (4), we can deduce the expression of the rotor flux as a function of the stator flux and rotor current:

$$\overrightarrow{\phi_r} = \frac{L_m}{L_s}\overrightarrow{\phi_s} + \sigma L_r \overrightarrow{I_r} \tag{12}$$

Substituting the expression of the rotor flux (12) into the expression of the rotor voltage (11), we get:

$$\overrightarrow{V_r} = \underbrace{\frac{L_m}{L_s}\left(\frac{d}{dt} - j\omega\right)\overrightarrow{\varphi_s}}_{A} + \underbrace{\left(R_r + \sigma L_r\left(\frac{d}{dt} - j\omega\right)\right)\overrightarrow{I_r}}_{B} \tag{13}$$

Analyzing the expression of the rotor voltage in eq. (13), we can see that it is decomposed into two terms, the first term A is the electromotive force (EMF) induced by the stator flux [2], when the current rotor is equal to zero $I_r = 0$ in the open circuit, the term A can be defined as:

$$\overrightarrow{V_{r0}} = \frac{L_m}{L_s}\left(\frac{d}{dt} - j\omega\right)\overrightarrow{\phi_s} \tag{14}$$

The second term B is the expression of the voltage dips in the rotor inductance σL_r and the rotor resistance R_r of the generator [17], when the current rotor is not equal to zero $I_r \neq 0$, the term B can be defined as:

$$\overrightarrow{V_{r1}} = \left(R_r + \sigma L_r\left(\frac{d}{dt} - j\omega\right)\right)\overrightarrow{I_r} \tag{15}$$

In this section, we assume that the DFIG operates in normal condition at the rated voltage V_{sn}, at $t = t_0$ a symmetrical partial voltage dip appears in the stator circuit whit a depth denoted d. Using eq. (13), and by neglecting the stator resistance R_s, the expression of the stator voltage and flux during symmetrical partial voltage drops becomes:

$$\overrightarrow{V_s} = \begin{cases} V_s e^{j\omega_s t} & t < t_0 \\ (1-d) V_s e^{j\omega_s t} \text{ When } & t \geq t_0 \end{cases} \tag{16}$$

$$\overrightarrow{\phi_s} = \begin{cases} \dfrac{V_s}{j\omega_s} e^{j\omega_s t} & \\ (1-d)\dfrac{V_s}{j\omega_s} e^{j\omega_s t} \text{ When } & \begin{matrix} t < t_0 \\ t \geq t_0 \end{matrix} \end{cases} \tag{17}$$

According to [28], when a symmetrical partial voltage drops appears on the electrical network, after t_0 the stator flux cannot change its value instantaneously, because the flux cannot have discontinuities, consequently, a second component appears to ensure it continuities and make it changes progressively. The expression of the stator flux during the fault can be rewritten as this form [17, 24]:

$$\overrightarrow{\varphi_s} = \underbrace{(1-d)\frac{V_s}{j\omega_s} e^{j\omega_s t}}_{\overrightarrow{\varphi_{sf}}} + \underbrace{d\frac{V_s}{j\omega_s} e^{-\frac{t}{\tau_s}}}_{\overrightarrow{\varphi_{sn}}} \tag{18}$$

The first term is the flux forced by the stator voltage connected to the grid under the voltage drops [3], is named "forced flux" ϕ_{sf}, the second term is the "natural flux" ϕ_{sn}, and τ_s is the stator flux time constant.

Substituting the eq. (18) into (14), the expression of the electromotive force EMF can be rewriting as the following form:

$$\overrightarrow{V_{r0}} = \frac{L_m}{L_s} V_s \left[s(1-d) e^{j\omega_s t} - \frac{d}{j\omega_s}\left(\frac{1}{\tau_s} + j\omega\right) e^{-\frac{t}{\tau_s}} \right] \tag{19}$$

By neglecting the term $1/\tau_s$ [17], the expression of the EMF can be simplified us:

$$\overrightarrow{V_{r0}} = \left(\underbrace{\frac{L_m}{L_s} s(1-d) V_s e^{j\omega_s t}}_{\overrightarrow{V_{rf}}} - \underbrace{\frac{L_m \omega}{L_s \omega_s} d V_s e^{-\frac{t}{\tau_s}}}_{\overrightarrow{V_{rn}}} \right) \tag{20}$$

Equation (20) is the sum of two terms, the first term V_{rf} is induced by the forced flux, its amplitude is very small and proportional to the slip s, as $s \approx 30\%$ and if the depth d was deep: its amplitude can be neglected. The second term is the voltage V_{rn} induced by the natural flux, its amplitude is proportional to the depth d.

If a severe voltage drop occurs, an important rotor voltage will be induced by the natural flux, which leads to suffering from over rotor currents limit, if this happens and the rotor side converter (RSC) is not good controlled the generator and the converter may even be damaged. So to perform the doubly fed induction generator operation under voltage drop and protect the RSC, the converter should be controlled in a good way.

3 Direct power control based-Backstepping technique

The principle of the nonlinear Backstepping technique is the use of a virtual control to decompose a complicated nonlinear system into several simpler subsystems, and each subsystem gives a reference for the next [12]. The system studied can achieve high performances and guarantee its stability, if the control method satisfies the conditions of Lyapunov stability.

The DPC based-Backstepping technique is proposed to ensure robust powers regulation under grid fault. Our controller is designed using the generator mathematical model. Substituting eq. (5) into (9), the expression of the stator powers as a function of the rotor and stator flux becomes:

$$P_s = \frac{k_r V_s}{\sigma L_s}\left(\frac{1}{k_r}\phi_{sq} - \phi_{rq}\right) \tag{21}$$

$$Q_s = \frac{k_r V_s}{\sigma L_s}\left(\frac{1}{k_r}\phi_{sd} - \phi_{rd}\right) \tag{22}$$

Using eq. (2) and (6), the expression of the rotor voltage becomes:

$$\begin{cases} V_{rd} = \dfrac{d\phi_{rd}}{dt} + \dfrac{R_r}{\sigma L_r}\phi_{rd} - \omega_r\phi_{rq} - \dfrac{R_r k_s}{\sigma L_r}\phi_{sd} \\ V_{rq} = \dfrac{d\phi_{rq}}{dt} + \dfrac{R_r}{\sigma L_r}\phi_{rq} + \omega_r\phi_{rd} - \dfrac{R_r k_s}{\sigma L_r}\phi_{sq} \end{cases} \quad (23)$$

According to eqs. (21), (22) and (23) the rotor voltages can be rewritten as follows:

$$\begin{cases} V_{rd} = -\dfrac{1}{\mu}\dfrac{dQ_s}{dt} - \alpha Q_s + \dfrac{1}{\mu}\omega_r P_s + \dfrac{1}{k_r}\dfrac{d\phi_{sd}}{dt} + \delta\phi_{sd} - \dfrac{1}{k_r}\omega_r\phi_{sq} \\ V_{rq} = -\dfrac{1}{\mu}\dfrac{dP_s}{dt} - \alpha P_s - \dfrac{1}{\mu}\omega_r Q_s + \dfrac{1}{k_r}\dfrac{d\phi_{sq}}{dt} + \delta\phi_{sq} + \dfrac{1}{k_r}\omega_r\phi_{sd} \end{cases} \quad (24)$$

Where:

$$\mu = \frac{k_r V_s}{\sigma L_s}; \alpha = \frac{R_r}{\sigma L_r \mu}; \delta = \frac{R_r(1-k_r k_s)}{\sigma L_r k_r}$$

The expressions of the rotor voltage in eq. (25) contain six terms, the first three terms present the normal operation of the DFIG, and the last three terms illustrate the variation of the flux during the grid fault.

$$\begin{cases} \dfrac{dQ_s}{dt} = -\mu\alpha Q_s + \omega_r P_s + \dfrac{\mu}{k_r}\dfrac{d\phi_{sd}}{dt} + \mu\delta\phi_{sd} - \dfrac{1}{k_r}\mu\omega_r\phi_{sq} - \mu V_{rd} \\ \dfrac{dP_s}{dt} = -\mu\alpha P_s - \omega_r Q_s + \dfrac{\mu}{k_r}\dfrac{d\phi_{sq}}{dt} + \mu\delta\phi_{sq} + \dfrac{1}{k_r}\mu\omega_r\phi_{sd} - \mu V_{rq} \end{cases} \quad (25)$$

From eq. (25), we can deduce that the rotor voltages are the variables to impose on the rotor side converter to control the active and reactive stator powers, the rotor voltage V_{rd} can control the reactive stator power Q_s, and the rotor voltage V_{rq} can control the active stator power P_s.

The reactive and active stator powers errors e_1 e_Q and e_P are defined by:

$$\begin{cases} e_Q = Q_s^* - Q_s \\ e_P = P_s^* - P_s \end{cases} \quad (26)$$

The derivative of the active and reactive stator powers errors gives:

$$\begin{cases} \dot{e_Q} = \dot{Q_s^*} - \dot{Q_s} \\ \dot{e_P} = \dot{P_s^*} - \dot{P_s} \end{cases} \quad (27)$$

Using Eq. (25), the derivative of the errors becomes:

$$\begin{cases} \dot{e_Q} = \dot{Q_s}* + \mu\alpha Q_s - \omega_r P_s - \dfrac{\mu}{k_r}\dot{\phi_{sd}} - \mu\delta\phi_{sd} + \dfrac{1}{k_r}\mu\omega_r\phi_{sq} + \mu V_{rd} \\ \dot{e_P} = \dot{P_s}* + \mu\alpha P_s + \omega_r Q_s - \dfrac{\mu}{k_r}\dot{\phi_{sq}} - \mu\delta\phi_{sq} - \dfrac{1}{k_r}\mu\omega_r\phi_{sd} + \mu V_{rq} \end{cases} \quad (28)$$

We use the Lyapunov candidate function, to reduce the errors:

$$v = \frac{1}{2}{e_Q}^2 + \frac{1}{2}{e_P}^2 \quad (29)$$

The derivative of the Lyapunov function gives:

$$\dot{v} = e_Q\dot{e_Q} + e_P\dot{e_P} \quad (30)$$

Substituting Eq. (28) into (30), the derivative of the Lyapunov function becomes:

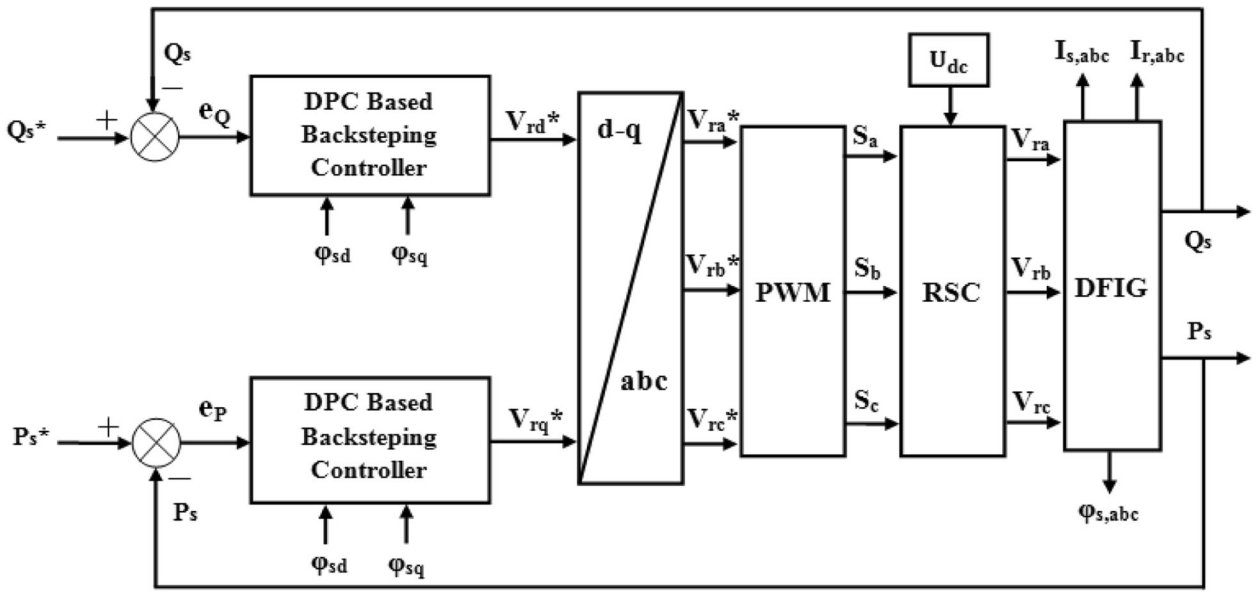

Fig. 3 The proposed DPC bloc diagram using the Backstepping approach

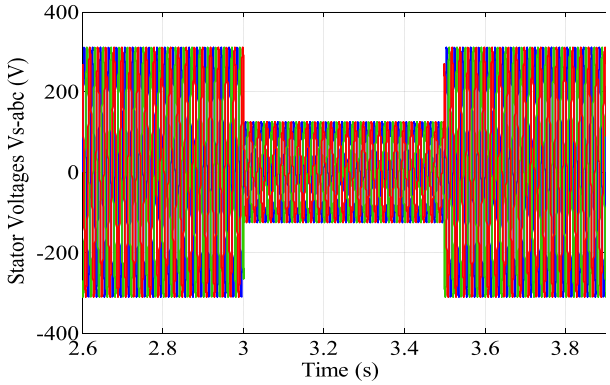

Fig. 4 Symmetrical Voltage dips of 60% ($\Delta V_s = 186$ V)

$$\begin{aligned}\dot{v} &= e_Q(\dot{Q}_s^* + \mu\alpha Q_s - \omega_r P_s - \frac{\mu}{k_r}\dot{\phi}_{sd} - \mu\delta\phi_{sd} \\ &+ \frac{1}{k_r}\mu\omega_r\phi_{sq} + \mu V_{rd}) + e_P(\dot{P}_s^* + \mu\alpha P_s \\ &+ \omega_r Q_s - \frac{\mu}{k_r}\dot{\phi}_{sq} - \mu\delta\phi_{sq} - \frac{1}{k_r}\mu\omega_r\phi_{sd} + \mu V_{rq}) \\ &= -k_Q {e_Q}^2 - k_P {e_P}^2\end{aligned} \tag{31}$$

To achieve good stator power regulation, the derivative of the Lyapunov candidate function should be negative and the gains k_Q and k_p must be positives parameters [29–31]:

$$\dot{v} = -k_Q {e_Q}^2 - k_P {e_P}^2 \le 0 \tag{32}$$

From Eqs. (31) and (32), we deduced the expression of the control rotor voltages variables V_{rd} and V_{rq}:

$$\begin{cases} V_{rd}^* = -\left(\frac{1}{\mu}\left(\dot{Q}_s^* + k_Q e_Q - \omega_r P_s\right) + \alpha Q_s\right) - \frac{1}{k_r}\left(\omega_r\phi_{sq} + \dot{\phi}_{sd}\right) + \delta\phi_{sd} \\ V_{rq}^* = -\left(\frac{1}{\mu}\left(\dot{P}_s^* + k_P e_P + \omega_r Q_s\right) + \alpha P_s\right) + \frac{1}{k_r}\left(\omega_r\phi_{sd} - \dot{\phi}_{sq}\right) + \delta\phi_{sq} \end{cases} \tag{33}$$

When the voltage dips occur on the supply terminal of the stator, the Backstepping controller must calculate the stator powers references to control the DFIG, perform its operation, and contribute to the return of the voltage to its rated value. In this situation, the expression of the maximum apparent stator power S_s is giving by [18]:

$$S_{s-\max} = I_{sn} V_{sn} \tag{34}$$

Where: V_{sn} and I_{sn} are the nominal stator voltage and current of the generator. By respecting the grid code, when the system control detects a voltage drops whit a depth $30\% < d < 80\%$ for a duration less than 1000 ms, the stator active and reactive powers references become:

$$\begin{cases} Q_s^* = -I_{sn} V_{sq}\left(1 - \frac{V_{sq}}{V_{sn}}\right) \\ P_s^* = 0 \end{cases} \tag{35}$$

The maximum of the reactive power Q_s injected into the electrical network is limited by this equation:

$$|\, Q_s^* \,| = S_{s\max} \tag{36}$$

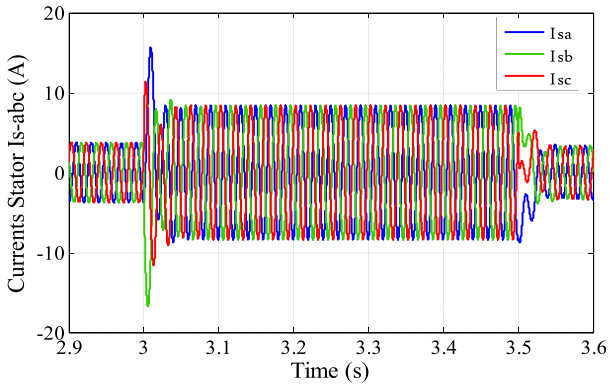

Fig. 5 Stator Currents $I_{s\text{-}abc}$ (A)

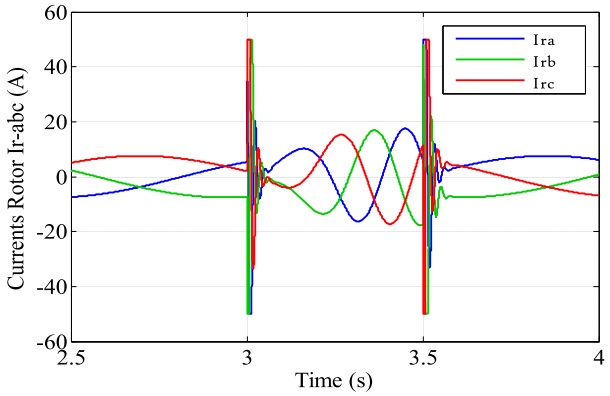

Fig. 6 Rotor Currents $I_{r\text{-}abc}$ (A)

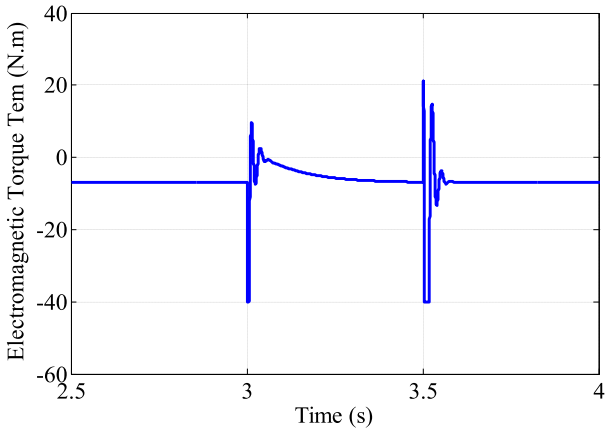

Fig. 7 Electromagnetic Torque T_{em} en (N.m)

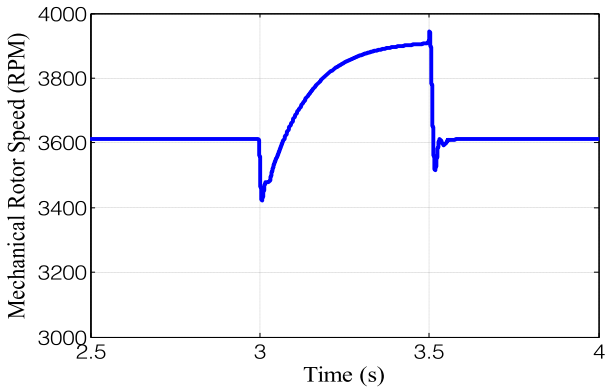

Fig. 8 Mechanical Rotor Speed Ω_m en (rpm)

Figure 3 illustrates the block diagram of our proposed DPC strategy using the nonlinear Backstepping technique.

4 Results and discussions

The simulation of the wind energy system under voltage dips was performed using Simulink® software, all simulations were realized whit a doubly fed induction aero-generator of 1.5 (kW) rated power, which the parameters of the generator and the wind turbine are given in the appendix. We suppose that the wind speed is constant during the voltage dips whit an average speed value v = 10 (m/s), because the duration of the fluctuation in the wind speed is bigger than the voltage drops [15]. The following tests giving below were done to analyze the dynamic behavior of the DFIG and ensure the robustness and performances of our proposed control method under symmetrical voltage sags:

- Behavior of the DFIG under voltage dips of 60%.
- DPC control based-Backstepping approach under voltage dips of 60%.
- Comparison whit the PI controller under symmetrical voltage.

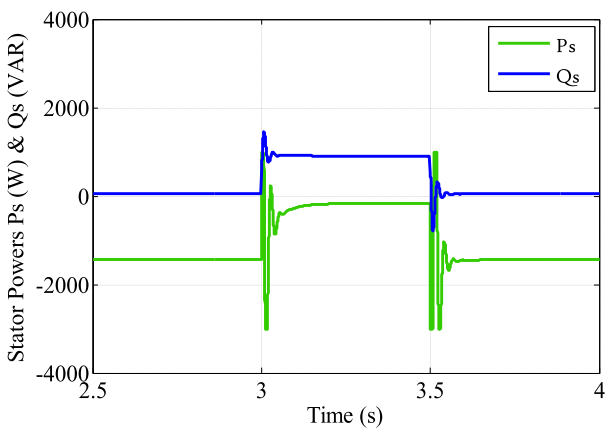

Fig. 9 Stator Powers Q (VAR) & P_s (W)

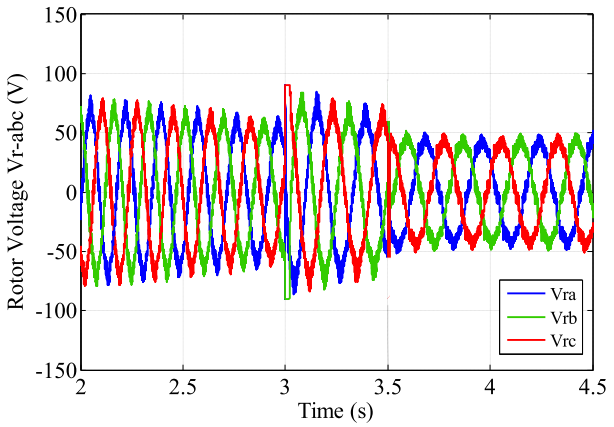

Fig. 10 Rotor Voltages $V_{r\text{-}abc}$ (V)

We apply to the supply terminal of the stator a symmetrical voltage drops whit a 60% depth for a duration of 500 (ms) appeared at t = 3 (s) and disappeared at t = 3.5 (s). Figure 4 shows the stator voltages $V_{s\text{-}abc}$ during the grid fault whit 60% of a voltage dips.

4.1 Behavior of the DFIG under voltage dips

We have modeled and simulated the aero-generator under Simulink environment, to study its dynamic behavior during the period of the fault. Figure 5 presents the response of the currents stator $I_{s\text{-}abc}$ injected into the network, as we see during the drop the currents increase and a high peak currents equal to $I_s = 3*I_{sn}$ occur at t = 3 (s) on the stator circuit, and the currents are re-established when the stator voltage return to its rated value at t = 3.5 (s). Figure 6 illustrates the evolution of the rotor currents $I_{r\text{-}abc}$ before, during and after the grid fault, we can see that during the voltage sags the frequency of the current rotor f_r increases, this change is caused by the acceleration of the DFIG, and a very high peaks currents equal to $I_r = 7*I_{rn}$ appear on the rotor circuit at the beginning and the end of the voltage dip, this

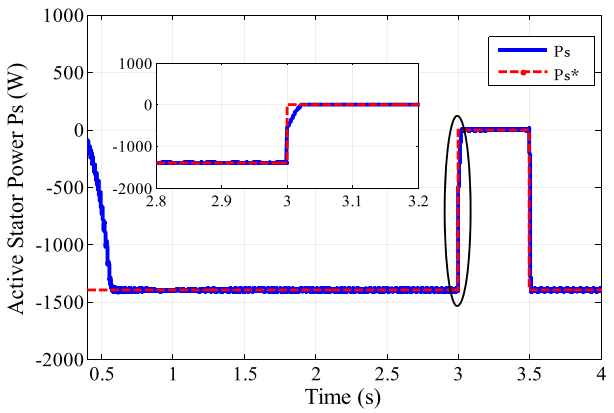

Fig. 11 Active Stator Power (W)

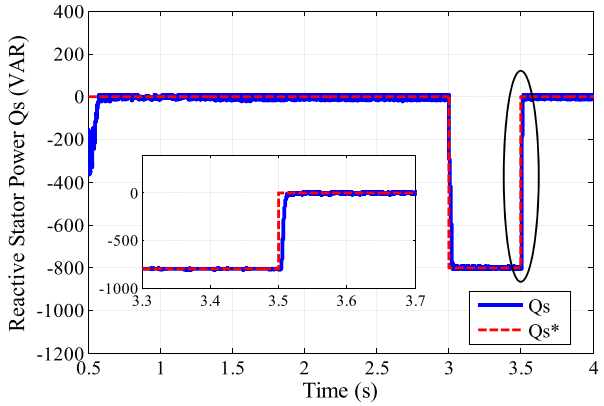

Fig. 12 Reactive Stator Power (VAR)

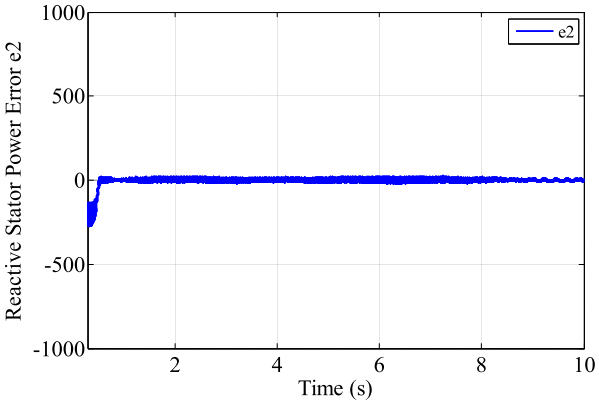

Fig. 14 Reactive Stator Power Error e2

over-current limit can damage the rotor side converter and the generator.

The electromagnetic torque is giving in Fig. 7, at the appearance of the dip t = 3 (s) the torque decreases and return to its value $T_{em} = -7$ (N.m) after 300 (ms), we can see that the torque oscillates at the beginning and the end of the network faults, that will cause a big press on the drive train. The mechanical rotor speed is presented in Fig. 8, the generator operates at the super-synchronous mode $\Omega_m > 3000$ (rpm), from t = 0 (s) to t = 3 (s) the rotor speed is constant and equal to 3620 (rpm), at t = 3 (s) the mechanical rotor speed is increased linearly from 3620 (rpm) to 3900 (rpm) during the period of the voltage dip. This increase in rotor speed is caused by the electromagnetic torque drop, since the DFIG is driven in rotation by the turbine; the electromagnetic torque of the generator presents the resistant torque of the turbine, so this decrease in torque causes the acceleration of the turbine speed, consequently, acceleration of the mechanical rotor speed.

Figure 9 shows the response of the stator powers, the reactive stator power Q_s changes from 0 (VAR) to 800 (VAR) at t = 3 (s), the generator consumes the reactive power to guarantee the magnetization of the DFIG during the period of the voltage drop, and returns to its initial value at t = 3.5 (s). The active stator power P_s becomes low and oscillates at the beginning and the end of the fault, at the return of the voltage to its nominal value, P_s and Q_s regain their values.

4.2 DPC based-Backstepping controller under voltage dips

The generator is operating under the maximum power point tracking (MPPT) algorithm without disturbances $P_s = -1450$ (W) and $Q_s = 0$ (VAR), the reactive stator power is kept null to have a unit power factor, the system control is enabled to detect the voltage dip, at t = 3(s) a sudden voltage sag appears at the supply terminal of the stator, consequently, the Backstepping controller calculates and generates the values of the rotor voltages references, Fig. 10 presents the evolution of the rotor

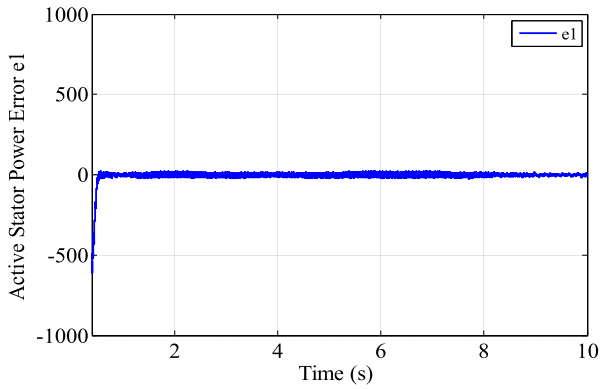

Fig. 13 Active Stator Power Error e_1

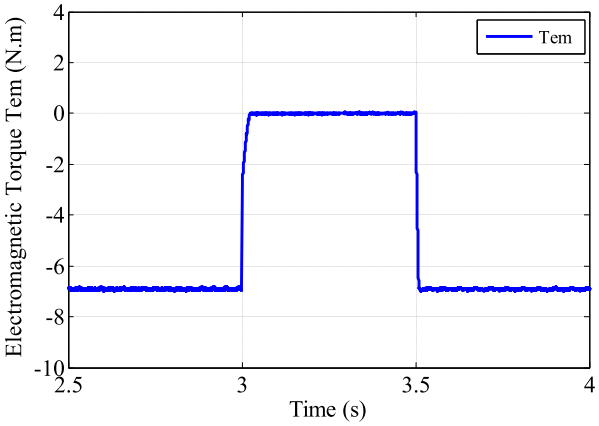

Fig. 15 Electromagnetic Torque T_{em} (N.m)

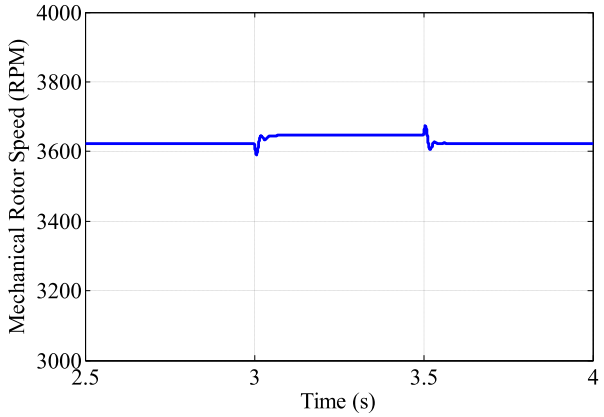

Fig. 16 Mechanical Rotor Speed Ω_m (rpm)

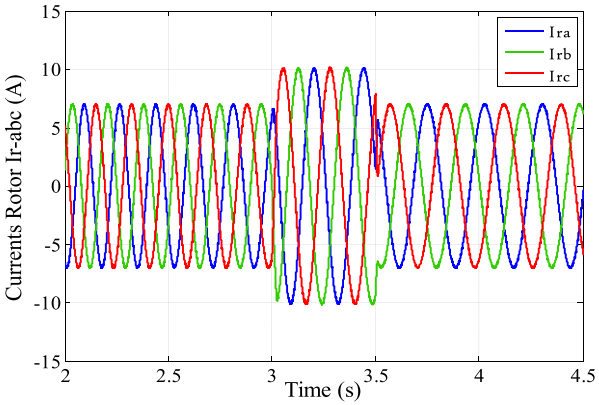

Fig. 18 Rotor Currents $I_{r\text{-}abc}$ (A)

voltages $V_{r\text{-}abc}$, we can see that the rotor voltages are sinusoidal and its amplitude increase from 60 (V) to 80 (V) during the faults.

The system control calculates the values of the active and reactive stator powers references, the active power P_s presented in Fig. 11 decreases from − 1450 (W) to 0 (W) to suppress the high peak currents, and the reactive stator power Q_s changes from 0 (VAR) to − 800 (VAR) (show Fig. 12), the reactive power is injected into the electrical grid to contribute to the return of the voltage to its nominal value, after the fault the aero-generator continue the production of the electrical power normally. As we see in Figs. 11 and 12 the tracking response is perfectly done during and after the fault, the Backstepping controller achieves the stator power references whit a fast response time, null steady-state errors and without power oscillations at the appearance and disappearance of the voltage drop. The powers errors e_1 and e_2 giving in Figs. 13 and 14 converge to zero that verify the good tracking performances of the Backstepping approach.

Figure 15 shows the response of the electromagnetic torque, during the period of the fault the torque converges to zero $T_{em} = 0$ (N.m) without oscillations and torque peaks at the appearance and disappearance of the fault, the mechanical rotor speed is giving in Fig. 16, during the drop of the voltage the rotor speed changes whit small fluctuations from 3620 (rpm) to 3650 (rpm) at $t = 3$ (s) and $t = 3.5$ (s) and becomes stable after cleaning the defect. As we see the DPC control has cleared the oscillations at the critical moments of the faults, which leads to perform the generator operation and protect the drive train of the system.

Figures 17 and 18 illustrate the response of the currents stator I_s and rotor I_r, respectively, it can be seen that the currents increase during the faults $I_s = 7$ (A) and $I_r = 10$ (A) in an acceptable way, without high peaks currents at the critical moments: the beginning and the end of the voltage sag, the limits of the

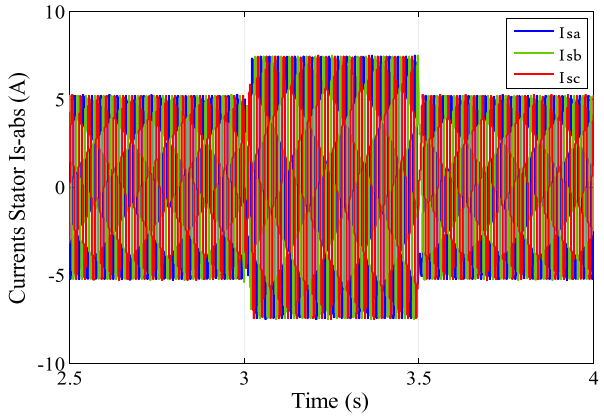

Fig. 17 Stator Currents $I_{s\text{-}abc}$ en (A)

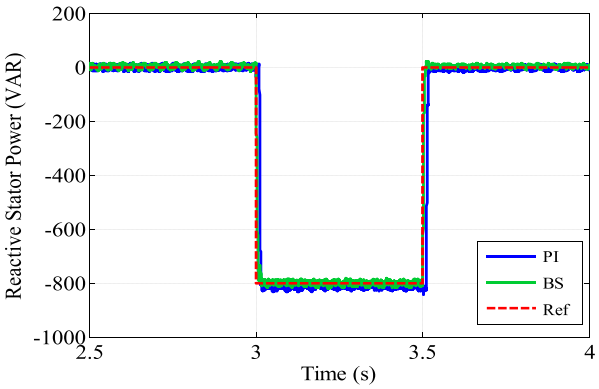

Fig. 19 Reactive Stator Power Qs (VAR)

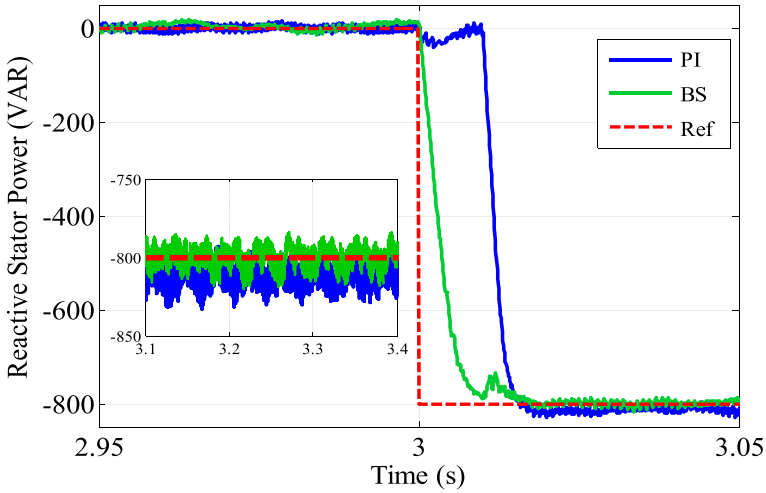

Fig. 20 Zoom on Reactive Stator Power Qs (VAR)

currents are respected: the stator current limit is $I_{s\text{-}max} = 7.5$ (A) and the rotor current limit is $I_{r\text{-}max} = 12.2$ (A). We can deduce that the direct power control (DPC) has achieved high efficiency and the objective of the control: suppress the peaks currents on the stator and rotor circuit, and contribute to the operation of the system studied, which confirm the performance and robustness of our proposed DPC control based-Backstepping technique.

4.3 Comparison whit the PI controller under symmetrical voltage dips

In order to verify our proposed DPC method based Backstepping controller, a comparison study was done whit the Proportional-Integral (PI) controller in terms of reference tracking under voltage dips. Figures 19 and 20 show the simulation results of the reactive stator power during a 60% of the voltage drop. As we see the Backstepping controller is robust, has faster response time and smaller steady state error compared to PI controller. Analyzing the results, we can conclude that this disturbance has almost no influence on the Backstepping controller (BS), but by using the PI controller the tracking response shows more undesirable results.

5 Conclusion

In this work a doubly fed induction aero-generator for a nominal power of 1.5 (kW) was modeled and simulated to investigate its dynamic behavior during balanced voltage dip, then a new DPC method based on the Backstepping technique was developed to perform the DFIG operation under grid fault, and contribute to the return of the voltage to its nominal value in the electrical grid. The Backstepping controller was designed using the generator mathematical model, in which the stator flux was admitted variants during all the period of the fault.

The simulations results under Simulink® software were satisfactory and the control performances were achieved using our proposed DPC approach, which can clear the high peaks currents on the stator and rotor circuit, without fluctuations in the stator powers at the beginning and the end of the grid fault, the system control is easy to be implemented in the hardware controller card, without using external hardware device, thus the DPC Based-Backstepping technique is an efficient, robust and suitable approach for controlling the DFIG connected to the electrical network.

As a future work, we will implement our system control in the dSPACE card to verify our proposed method by experiments.

6 Appendix

Table 1 DFIG A4222 parameters

Symbol	Quantity	Value (unit)
P_n	Rated Power	1500 W
V_{sn}	Rated Stator Voltage	220 / 380 V
I_{sn}	Stator Current	5.2 A
I_{rn}	Rotor Current	8.5 A
p	Number of pole pairs	1
R_s	Stator Resistance	1.18 Ω
R_r	Rotor Resistance	1.66 Ω
L_m	Mutual Inductance	0.17 H
L_s	Stator Inductance	0.20 H

Table 2 Wind Turbine parameters

Symbol	Quantity	Value (unit)
R	Turbine Radius	1 m
G	Multiplier	2
J	Total Inertia	0.04 (kg.m^2)
C_f	Coefficient of frictions	0.007
ρ	Air Density	1.22 (kg/m^3)

Abbreviations

d: Depth of the Voltage drop; $e_{Q,P}$: Reactive active power errors; $I_{s,r}$: Stator and rotor current; $k_{Q,P}$: Backstepping Controller gains; L_m: Maximum of the mutual inductance; $L_{s,r}$: Stator and rotor Inductance; p: Number of pole pair; P_s: Stator active power; Q_s: Stator reactive power; $R_{s,r}$: Stator and rotor resistance; s: Slip; S_s: Stator apparent power; T_{em}: Electromagnetic torque; V_n,I_n: Nominal voltage and current; $V_{s,r}$: Stator and rotor voltage; σ: Linkage coefficient; τ_s: Stator flux time constant; Φ_s: Stator and rotor flux; $_{s,r}$: Stator and rotor pulsation

Acknowledgements

Not applicable.

Authors' contributions

SM as a corresponding author, proposed the structure and wrote the manuscript, modeled the WECS and the proposed DPC method using the MATLAB software. AE, TN and BBI as supervisors contributed to perform and revise the manuscript. All authors read and approve the manuscript.

Funding

The research work is not supported by any funding agency.

Availability of data and materials

Data sharing not applicable to this article as no datasets were generated or analyzed during the current study.

Competing interests

The authors declare that they have no competing interests.

Author details

[1]Research Center of Engineering and Health Sciences and Technologies from ENSET, Mohammed V University, Rabat, Morocco. [2]Research Center of Engineering and Health Sciences and Technologies from ENSIAS, Mohammed V University, Rabat, Morocco. [3]Electromechanical Engineering Department of ENSAM, Moulay Ismaïl University, Meknès, Morocco.

Received: 20 September 2019 Accepted: 10 December 2019
Published online: 19 January 2020

References

1. Gholizadeh, M., Tohidi, S., Oraee, A., & Oraee, H. (2018). Appropriate crowbar protection for improvement of brushless DFIG LVRT during asymmetrical voltage dips. *International Journal of Electrical Power & Energy Systems, 95*, 1–10.
2. Noureldeen, O., & Hamdan, I. (2018). A novel controllable crowbar based on fault type protection technique for DFIG wind energy conversion system using adaptive neuro-fuzzy inference system. *Protection and Control of Modern Power Systems, 3*(1), 35.
3. López, J., Gubía, E., Olea, E., Ruiz, J., & Marroyo, L. (2009). Ride through of wind turbines with doubly fed induction generator under symmetrical voltage dips. *IEEE Transactions on Industrial Electronics, 56*(10), 4246–4254.
4. Mensou, S., Essadki, A., Minka, I., Nasser, T., Idrissi, B. B., & Bentarla, L. (2019). Performance of a vector control for DFIG driven by wind turbine: Real time simulation using DS1104 controller board. *International Journal of Power Electronics and Drive Systems, 10*(2), 1003–1013.
5. El Ouanjli, N., Motahhir, S., Derouich, A., El Ghzizal, A., Chebabhi, A., & Taoussi, M. (2019). Improved DTC strategy of doubly fed induction motor using fuzzy logic controller. *Energy Reports, 5*, 271–279.
6. Yang, B., et al. (2016). Nonlinear maximum power point tracking control and modal analysis of DFIG based wind turbine. *International Journal of Electrical Power & Energy Systems, 74*, 429–436.
7. Yang, B., et al. (2018). Robust sliding-mode control of wind energy conversion systems for optimal power extraction via nonlinear perturbation observers. *Applied Energy, 210*, 711–723.
8. Yang, B., et al. (2017). Perturbation estimation based robust state feedback control for grid connected DFIG wind energy conversion system. *International Journal of Hydrogen Energy, 42.33*, 20994–21005.
9. Ayyarao, T. S. (2019). Modified vector controlled DFIG wind energy system based on barrier function adaptive sliding mode control. *Protection and Control of Modern Power Systems, 4*(1), 4.
10. Boubzizi, S., Abid, H., & Chaabane, M. (2018). Comparative study of three types of controllers for DFIG in wind energy conversion system. *Protection and Control of Modern Power Systems, 3*(1), 21.
11. Kaloi, G. S., Wang, J., & Baloch, M. H. (2016). Active and reactive power control of the doubly fed induction generator based on wind energy conversion system. *Energy Reports, 2*, 194–200.
12. Mensou, S., Essadki, A., Nasser, T., & Idrissi, B. B. (2017). An efficient nonlinear Backstepping controller approach of a wind power generation system based on a DFIG. *International Journal of Renewable Energy Research, 7*(4), 1520–1528.
13. Mensou, S., Essadki, A., Nasser, T., Idrissi, B. B., & Tarla, L. B. (2020). Dspace DS1104 implementation of a robust nonlinear controller applied for DFIG driven by wind turbine. *Renewable Energy Elsevier, 147*, 1759–1771.
14. Jacomini, R. V., & Sguarezi Filho, A. J. (2019). Finite control set applied to the direct power control of a DFIG operating under voltage sags. *IEEE Transactions on Sustainable Energy, 10*(2), 952–960.
15. Chakib, R., Cherkaoui, M., & Essadki, A. (2015). Stator flux control by active disturbance rejection control for DFIG wind turbine during voltage dip. *International Journal of Circuits Systems and Signal Processing, 9*, 281–288.
16. Jacomini, R. V., & Sguarezi Filho, A. J. (2018). Direct power control strategy to enhance the dynamic behavior of DFIG during voltage sag. *Proceeding of the 7th International Conference on Renewable Energy Research and Applications*, 194–198.
17. Xiao, S., Yang, G., Zhou, H., & Geng, H. (2013). A LVRT control strategy based on flux linkage tracking for DFIG-based WECS. *IEEE Transactions on Industrial Electronics, 60*(7), 2820–2832.
18. Franco, R., Capovilla, C. E., Jacomini, R. V., Altana, J. A. T., & Filho, A. J. S. (2014). A deadbeat direct power control applied to doubly-fed induction aerogenerator under normal and sag voltages conditions. *Proceeding of the 40th Annual Conference of the IEEE Industrial Electronics Society*, 1906–1911.
19. Morren, J., & de Haan, S. W. H. (2005). Ride through of wind turbines with doubly-fed induction generator during a voltage dip. *IEEE Transactions on Energy Conversion, 20*(2), 435–441.
20. Rahimi, M., & Parniani, M. (2010). Grid-fault ride-through analysis and control of wind turbines with doubly fed induction generators. *Electric Power Systems Research, 80*, 184–195.
21. Qiao, W., Venayagamoorthy, G. K., & Harley, R. G. (2009). Real-time implementation of a STATCOM on a wind farm equipped with doubly fed induction generators. *IEEE Transactions on Industrial Applications, 45*(1), 98–107.
22. Muni Reddy, G., & Gowri Manohar, T. (2018). Fuzzy logic controller based STATCOM for grid connected wind turbine system. *International Journal of Renewable Energy Research, 8*(2), 702–713.
23. Thirupathaiah, M., Venkata Prasad, P., & Ganesh, V. (2018). Enhancement of power quality in wind power distribution system by using hybrid PSO-firefly based DSTATCOM. *International Journal of Renewable Energy Research, 8*(2), 1138–1154.
24. Solís-Chaves, J. S., Barreto, M. S., Salles, M. B., Lira, V. M., Jacomini, R. V., & Sguarezi Filho, A. J. (2017). A direct power control for DFIG under a three phase symmetrical voltage sag condition. *Control Engineering Practice, 65*, 48–58.
25. Francisco, K., Lima, A., Luna, A., Rodriguez, P., Watanabe, E. H., & Blaabjerg, F. (2010). Rotor voltage dynamics in the doubly fed induction generator during grid faults. *IEEE Transactions on Power Electronics, 25*(1), 118–130.
26. Kharchouf, I., Essadki, A., & Nasser, T. (2017). Wind system based on a doubly fed induction generator: Contribution to the study of electrical energy quality and continuity of service in the voltage dips event. *International Journal of Renewable Energy Research, 7*(4), 1892–1900.
27. Jeong, H. G., Ro, H. S., & Lee, K. B. (2013). A control scheme of the low voltage ride through in wind turbines using a direct power control based

on a sliding mode control. *Proceeding of the International Symposium on Industrial Electronics*, 1–6.
28. Lopez, J., Sanchis, P., Roboam, X., & Marroyo, L. (2007). Dynamic behavior of the doubly fed induction generator during three-phase voltage dips. *IEEE Transactions on Energy Conversion, 22*(3), 709–717.
29. Mensou, S., Essadki, A., Nasser, T., & Idrissi, B. B. (2017). A robust speed control of a doubly fed induction generator using in WECS by the nonlinear Backstepping controller. *Proceeding of the 3rd International Conference on Electrical and Information Technologies*, 1–6.
30. Mensou, S., Essadki, A., Minka, I., Nasser, T., & Idrissi, B. B. (2017). Backstepping controller for a variable wind speed energy conversion system based on a DFIG. In *Proceeding of the 5th international renewable and sustainable energy conference*.
31. Mensou, S., Essadki, A., Minka, I., Nasser, T., & Idrissi, B. B. (2019). Control and hardware simulation of a doubly fed induction aero-generator using dSPACE card. In *Proceeding of the 2nd International Conference of Computer Science and Renewable Energies*.